Research Square

Preprints are preliminary reports that have not undergone peer review.
They should not be considered conclusive, used to inform clinical practice,
or referenced by the media as validated information.

Berberine Ameliorates Primary Biliary Cholangitis by Modulating the Gut–Liver Axis and Attenuating Cholangiocyte Oxidative Stress in Murine Models and Human Organoids

Yechen Wu
First Affiliated Hospital Zhejiang University
Yuxi Zhao
First Affiliated Hospital Zhejiang University
Kaicen Wang
First Affiliated Hospital Zhejiang University
Tinglei Song
First Affiliated Hospital Zhejiang University
Pengyu Yin
First Affiliated Hospital Zhejiang University
Fengjiao Wang
First Affiliated Hospital Zhejiang University
Jiali Ni
First Affiliated Hospital Zhejiang University
Yulan Pan
First Affiliated Hospital Zhejiang University
Qianhan Xie
First Affiliated Hospital Zhejiang University
Andreas Teufel
Universität Greifswald
Lanjuan Li
First Affiliated Hospital Zhejiang University
Yanfei Chen
chenyf_zju@zju.edu.cn

First Affiliated Hospital Zhejiang University

Research Article

Keywords: Gut microbiota, Primary Biliary Cholangitis, Organoid, Cholangiocyte, Berberine

Posted Date: August 31st, 2026

DOI: https://doi.org/10.21203/rs.3.rs-10116628/v1

License: This work is licensed under a Creative Commons Attribution 4.0 International License.
Read Full License

Additional Declarations: No competing interests reported.

Abstract

Background

Primary biliary cholangitis (PBC) is a chronic autoimmune cholestatic liver disease characterized by progressive destruction of intrahepatic bile ducts, resulting in liver inflammation and fibrosis. Despite ursodeoxycholic acid as the standard therapy, a substantial proportion of patients show incomplete responses. Berberine hydrochloride (BBR), a bioactive alkaloid derived from traditional Chinese medicine, exhibits anti-inflammatory, antioxidant, and microbiota-modulating properties. While BBR has shown therapeutic potential in primary sclerosing cholangitis, its efficacy and underlying mechanisms in PBC remain largely unexplored.

Purpose

This study was designed to explore the therapeutic potential of BBR and elucidate its underlying mechanisms in the treatment of PBC.

Methods

We established a murine PBC model by intraperitoneal injection of 2-octynoic acid–BSA. BBR was then administered to the mice via oral gavage. Liver injury and fibrosis were evaluated using hematoxylin and eosin staining, Sirius red staining, immunohistochemistry, reverse transcription-quantitative PCR (RT-qPCR), liver function tests, and transcriptomic analysis. Gut microbiota composition was analyzed by 16S rRNA gene sequencing. To address how BBR protects biliary epithelial cells from oxidative stress injury, we employed an in vitro H_2O_2-induced injury model in human bile-derived cholangiocyte organoids. Mechanistic insights were then sought through transcriptomic and Olink proteomic analyses, with key findings validated by RT-qPCR, immunofluorescence, transmission electron microscopy, and ELISA.

Results

BBR markedly ameliorated liver inflammation and fibrosis in PBC mice and significantly modulated gut microbiota composition. Mechanistically, these effects were associated with the upregulation of bile secretion–related pathways,peroxisome proliferator-activated receptor and glutathione metabolic pathways. In cholangiocyte organoids, BBR attenuated oxidative stress–induced injury by suppressing pro-inflammatory cytokine signaling, restoring mitochondrial function, and enhancing metabolic adaptation.

Conclusion

These findings indicate that BBR exerts protective effects against PBC by targeting the gut–liver axis and cholangiocyte oxidative stress responses, supporting its potential as a promising therapeutic candidate for PBC.

1. Introduction

Primary biliary cholangitis (PBC) is an autoimmune disease characterized by chronic non-suppurative destructive cholangitis. Without intervention, PBC can lead to fibrosis, cirrhosis, and liver failure. The global annual incidence is approximately 1.76 per 100,000, with a prevalence of 14.6 per 100,000, both figures showing an upward trend. PBC is characterized by the progressive destruction of interlobular bile ducts. In this process, biliary epithelial cells are not only the primary targets of immune-mediated attack but also key active participants in the initiation and progression of the disease. Current evidence indicates that biliary epithelial cell injury in PBC is not driven by a single immune mechanism; rather, it results from the synergistic effects of autoimmune responses, oxidative stress, and disruption of intestinal homeostasis (Huang et al., 2023; Tanaka et al., 2024; Zheng et al., 2024).

The microbiome plays a critical role in maintaining immune homeostasis. In PBC, microbes are thought to trigger autoimmune responses through molecular mimicry mechanisms. For instance, recurrent urinary tract infections have been linked to the onset of PBC (Tanaka et al., 2019), with the mechanism involving *Escherichia coli* PDC-E2 antigens breaking immune tolerance to mitochondrial autoantigens (Yang et al., 2022). Recent studies have shown that PBC patients exhibit reduced gut microbiome diversity (Tang et al., 2018), with a decrease in beneficial bacteria and an increase in opportunistic pathogens (Lv et al., 2016). Further studies demonstrated that compared to PBC mice receiving fecal microbiota transplants (FMT) from healthy donors, those receiving FMT from PBC patients developed more severe liver damage and activation of immune-related pathways (Jiang et al., 2024). Additionally, the gut microbiota is associated with PBC treatment, as ursodeoxycholic acid (UDCA) has been shown to improve the gut microbiota structure (Tang et al., 2018), while patients with lower abundances of Clostridia taxa exhibit poorer responses to UDCA (Liu et al., 2025). These findings highlight the crucial role of the gut microbiome in the onset and treatment of PBC.

Current therapeutic options for PBC include UDCA and peroxisome proliferator-activated receptor (PPAR) agonists (Tanaka et al., 2024). However, 20–50% of patients show inadequate responses to UDCA, and approximately 9.1% of UDCA-treated PBC patients develop severe cirrhosis-related complications (Harms et al., 2018). In recent years, PPAR agonists such as seladelpar and elafibranor have been successful in double-blind phase III randomized controlled trials and were approved by the U.S. Food and Drug Administration in 2024 for PBC treatment (Komori & Kugiyama, 2025), although their long-term efficacy and safety require further evaluation. On the other hand, the farnesoid X receptor (FXR) agonist obeticholic acid has been restricted due to reported risks of liver function deterioration, and its use in decompensated cirrhosis has been limited (Lindor et al., 2022), with voluntary market withdrawal in the U.S. under FDA mandate in September 2025. Thus, there is an urgent need for safer and more effective treatment strategies for PBC.

Berberine (BBR), a quaternary ionic isoquinoline alkaloid predominantly derived from the stems and roots of *Berberis* species, has been widely recognized for its safety in traditional medicine(Chen et al., 2025; Li et al., 2023). BBR possesses diverse biological activities, including anti-inflammatory, antioxidant, and anti-tumor effects, while also modulating the gut microbiota and improving metabolic disturbances and intestinal inflammation, thereby demonstrating dual therapeutic effects (Chen et al., 2025; Habtemariam, 2020; Li et al., 2023).The liver is the primary target organ for BBR, with its metabolites reaching the highest concentrations in the liver after absorption (Habtemariam, 2020). Previous studies have shown that BBR significantly improves liver injury in animal models of autoimmune hepatitis and primary sclerosing cholangitis (PSC) (Hameed et al., 2024; Wang et al., 2024; Yao et al., 2023; Zhang et al., 2020). BBR exerts its biological activities through multiple mechanisms, such as acting as a ligand for the FXR receptor to regulate bile acid homeostasis (Hameed et al., 2024); its antimicrobial properties reduce bacteria that produce bile salt hydrolases, which increases taurocholic acid levels and further enhances FXR activation in the gut (Tian et al., 2019); additionally, BBR activates the PPAR pathway to exert its antioxidant effects (Owumi et al., 2024; Yu et al., 2016).

Given the core roles of bile acid dysregulation, cholangiocyte injury, and gut microbiota imbalance in the pathogenesis of PBC, BBR represents a promising but underexplored therapeutic candidate for PBC. This study constructs a murine PBC model to systematically observe the effects of BBR on disease progression, while using human bile-derived cholangiocyte organoids to explore its impact on cholangiocyte cells and its potential mechanisms. The findings aim to provide key preclinical evidence for the clinical application of BBR in the treatment of PBC.

2. Materials and methods

Details of the omics methods can be found in the Supplementary Materials, and the materials and experimental instruments used in this work are listed in Supplementary Tables S1 and S2, respectively. All animal experiments reported herein were performed in strict accordance with the ARRIVE guidelines 2.0 for reporting animal research. The raw sequence data reported in this paper have been deposited in the Genome Sequence Archive in National Genomics Data Center, China National Center for Bioinformation / Beijing Institute of Genomics, Chinese Academy of Sciences (GSA: CRA046838 and HRA016780) that are publicly accessible at https://ngdc.cncb.ac.cn/gsa.

2.1 Establishment of a murine PBC model and BBR intervention

Animal procedures were reported in accordance with ARRIVE Guidelines 2.0; completed ARRIVE 2.0 checklist is attached as supplementary file (Supplementary table S5). Six-week-old female C57BL/6J mice, sourced from the Zhejiang Provincial Experimental Animal Center, were kept in specific pathogen-free conditions at 22 ± 2°C and 50 ± 10% humidity, with a 12-hour light/dark cycle. Mice were provided with free access to food and water. After one week of acclimatization, a total of 18 mice were randomly assigned into three groups (n = 6 per group): the Ctrl group, the PBC group, and the BBR group. This

study was approved by the Clinical Research Ethics Committee of the First Affiliated Hospital, Zhejiang University School of Medicine (No. 2026–004).

The PBC model was established according to a previously described protocol (Wakabayashi et al., 2008). Briefly, 200 μg of 2-octynoic acid–bovine serum albumin conjugate (2OA-BSA) was dissolved in 100 μL saline and emulsified with an equal volume of complete Freund's adjuvant (CFA). An incomplete Freund's adjuvant (IFA) emulsion was prepared using the same procedure. Mice in the PBC and BBR groups received an intraperitoneal injection of 200 μg 2OA-BSA/CFA emulsion together with 100 ng pertussis toxin on day 1, followed by an additional intraperitoneal injection of 100 ng pertussis toxin on day 3. From day 15 onward, mice were boosted weekly by intraperitoneal injection of 200 μg 2OA-BSA/IFA emulsion, and the immunization protocol was continued for 8 weeks. Prior to blood and tissue harvesting, all mice underwent intraperitoneal anesthesia with pentobarbital sodium solution (50 mg/kg body weight, concentration: 50 mg/mL, dissolved in sterile normal saline). After complete loss of pain and righting reflex, mice were euthanized via cervical dislocation as the primary humane endpoint, followed by secondary thoracotomy to confirm death. No inhalation anesthetics were used in this study. All euthanasia procedures complied with institutional animal welfare guidelines.

BBR was dissolved in saline at a concentration of 5 mg/mL. Starting from day 3, mice in the BBR group were administered BBR via oral gavage at 50 mg/kg every other day. Mice in the Ctrl and PBC groups received equal volumes of saline. After 9 weeks of treatment, mice were euthanized, and samples including whole blood, liver tissue, and colonic contents were collected. Whole blood was centrifuged at 3,000 rpm for 10 min at 4°C to collect serum, and other samples were stored at − 80°C for subsequent analysis.

2.2 Liver histology and immunohistochemistry

Liver tissues were fixed in 4% paraformaldehyde for 48 h, then cleared with xylene and dehydrated through graded ethanol solutions. The tissues were embedded in paraffin and sectioned into 4 μm-thick slices. After hematoxylin and eosin (H&E) and Sirius Red staining, the sections were mounted with neutral resin for histological analysis.

Embedded sections were further processed for immunohistochemistry (IHC). After routine deparaffinization and rehydration, antigen retrieval was performed using microwave heating. Sections were rinsed with phosphate-buffered saline (PBS) and incubated with 3% H_2O_2 at room temperature for 25 min, followed by additional PBS washes. The sections were then incubated with 3% bovine serum albumin (BSA) for 30 min at room temperature and incubated overnight at 4°C with primary antibodies in a humidified chamber.

On the following day, sections were washed with PBS and incubated with a secondary antibody at room temperature for 50 min. After thorough washing with PBS, immunoreactivity was visualized using 3,3'-diaminobenzidine, and nuclei were counterstained with hematoxylin. Sections were subsequently dehydrated through graded ethanol, cleared in xylene, and mounted with neutral resin. Whole-slide

images were acquired using an automated digital slide scanner (KF-PRO-120, KFBIO, China). Positive staining areas were quantified using ImageJ software. Investigators responsible for histological assessment, immunohistochemical image quantification, and data analysis were blinded to group allocation.

2.3 Liver function analysis

Serum liver function parameters were measured using an automated biochemical analyzer (LW C400, Landwind, Shenzhen, China).

2.4 Establishment and intervention of human bile-derived cholangiocyte organoids

Organoid establishment is described in detail in the Supplementary Materials.

Cholangiocyte organoids at passage 2 were subjected to experimental intervention on day 3 of culture and randomly assigned to three groups: Ctrl, H_2O_2 and BBR groups. The Ctrl group was treated with an equal volume of PBS. Organoids in the H_2O_2 group were treated with 2.5 μM H_2O_2, whereas those in the BBR group received combined treatment with 2.5 μM H_2O_2 and BBR (1%).

During the intervention period, organoid morphological changes were documented by microscopy every two days for a total duration of 7 days. On day 7, culture supernatants were collected and stored at −80°C for Olink-based proteomic and cytokine analysis, while organoids were harvested for Real-time quantitative PCR (RT-qPCR) and transcriptome analysis. All experiments were independently repeated three times.

2.5 Histological staining and Immunofluorescence analysis of organoids

Organoids were collected using Cell Recovery Solution. H&E staining was performed as described above. Organoids were subjected to Acridine Orange/Propidium Iodide (AO/PI) staining, phalloidin staining, and senescence-associated β-galactosidase (SA-β-gal) using the respective reagents according to the manufacturers' protocols.

Multiplex immunofluorescence staining was conducted on paraffin-embedded sections using a sequential tyramide signal amplification (TSA) protocol. Sections were deparaffinized and rehydrated, followed by heat-mediated antigen retrieval in EDTA buffer (pH 9.0). After blocking with 10% normal goat serum, samples were incubated with primary antibodies at 4°C overnight and then with HRP-conjugated secondary antibodies. Signal development was performed using TSA reagents according to the manufacturer's instructions. After each staining cycle, antibody complexes were stripped by microwave treatment in citrate buffer, while the covalently deposited TSA fluorophores were retained. The staining procedure was repeated sequentially for additional targets. Nuclei were counterstained with DAPI, and sections were mounted with antifade medium and kept at 4°C in the dark prior to imaging.

2.6 Transmission Electron Microscopy (TEM) Analysis of Organoids

Organoids were fixed with 2.5% glutaraldehyde at 4°C, followed by post-fixation with 1% osmium tetroxide. Samples were dehydrated through a graded ethanol series, transferred to acetone, and embedded in epoxy resin. Ultrathin sections (60–80 nm) were prepared and stained with uranyl acetate and lead citrate. The ultrastructure of organoids was examined and imaged using a TEM (Hitachi, Tokyo, Japan).

2.7 Cytokine measurement in cholangiocyte organoids

Supernatants of cholangiocyte organoids stored at − 80°C were thawed and collected. The concentrations of tumor necrosis factor-α (TNF-α), interleukin (IL)-6, C-X-C motif chemokine ligand (CXCL)-1, CXCL2, and CXCL10 were quantified using enzyme-linked immunosorbent assay (ELISA) kits according to the manufacturer' instructions.

2.8 RT-qPCR analysis

Total RNA was extracted from liver tissues and cholangiocyte organoids using the RNeasy Plus Mini Kit (Qiagen, CA, USA) following the manufacturer's instructions. The RNA was reverse transcribed into cDNA using the PrimeScript RT Reagent Kit with gDNA Eraser (Takara, Kusatsu, Japan). Real-time PCR was then conducted using TB Green Premix Ex Taq (Takara) on a real-time PCR system. Relative mRNA expression levels of target genes were calculated by the $2 - \Delta\Delta Ct$ method, with GAPDH as the internal control. Primer sequences are listed in Table S3.

Statistical analysis

Data were analyzed using GraphPad Prism 9 (GraphPad Software Inc., La Jolla, CA). Results are presented as mean ± SEM. Normality was assessed using the Shapiro–Wilk test. For two-group comparisons, an unpaired two-tailed Student's t-test was used for normally distributed data. For multiple comparisons, normally distributed data were analyzed by one-way ANOVA followed by Tukey's post hoc test, whereas non-normally distributed data were analyzed using the Kruskal–Wallis test followed by Dunn's post hoc test. A two-tailed P value < 0.05 was considered statistically significant. Statistical significance is indicated as $*p < 0.05$, $**p < 0.01$, and $***p < 0.001$.

3. Results

3.1 BBR attenuates hepatic inflammation and fibrosis in a murine PBC model

As shown in Fig. 1A, to verify the successful establishment of the PBC model and assess the effects of BBR intervention, histopathological analysis was performed on mouse liver tissue at week 9. H&E

staining results revealed that the portal areas in the PBC group mice were enlarged, accompanied by extensive infiltration of inflammatory cells, mainly neutrophils and macrophages (Fig. 1B). Sirius Red staining showed noticeable collagen fiber deposition around the portal areas, with some arranged in a star-like pattern. These pathological changes were consistent with typical features of PBC. In contrast, the BBR intervention group showed reduced inflammatory infiltration in the portal areas and alleviated collagen deposition (Fig. 1C). Immunohistochemical results showed that in the PBC group, cytokeratin 19 (CK19)-positive bile ducts in the portal areas were surrounded by inflammatory cells, with some regions showing reactive hyperplasia of CK19-positive bile ducts, while the intervention group exhibited suppressed reactive hyperplasia of bile ducts. IL-6 positive signals were mainly distributed in the cytoplasm of hepatocytes, with strong patchy staining in the PBC group, while weak, scattered expression was observed in the BBR group. P21 expression in the PBC group was primarily localized to inflammatory cells in the portal areas and some fragmented necrotic hepatocytes, whereas expression was significantly reduced in the intervention group (Fig. 1D).

Liver function tests revealed significantly higher levels of aspartate aminotransferase (AST), alanine aminotransferase (ALT), and gamma-glutamyl transferase (GGT) in the PBC group compared to the Ctrl group. After BBR treatment, AST and GGT levels decreased significantly, while ALT levels showed no significant change (Fig. 1E). RT-qPCR further demonstrated that the hepatic mRNA levels of α-smooth muscle actin, CXCL6, CXCL10, IL-6, IL-8, p16, and TNF-α in the PBC group were markedly upregulated, while the expression of these genes was significantly reduced following BBR treatment (Fig. 1F).

3.2 BBR restores metabolic pathways and suppresses inflammatory signaling in PBC livers

Principal component analysis (PCA) of liver transcriptome profiles showed distinct clustering of the Ctrl, PBC, and BBR groups (Fig. 2A). Compared with the PBC group, BBR treatment resulted in 179 upregulated and 112 downregulated genes significantly (Fig. 2B–C). KEGG pathway enrichment analysis indicated that BBR-upregulated genes were mainly associated with drug metabolism, whereas downregulated genes were predominantly enriched in cell cycle– and NF-κB–related pathways (Fig. 2D). GSEA further revealed that BBR significantly upregulated pathways related to PPAR signaling, bile secretion, oxidative phosphorylation, and glutathione metabolism, while suppressing neutrophil extracellular trap formation and complement and coagulation cascades (Fig. 2E). Notably, within the PPAR signaling pathway, PPAR-α and several bile secretion related genes (Sult2a8, Sult2a3, and Abcb1a), as well as glutathione metabolism–related genes (Gsta2, Gstt2, and Gsta1), were significantly upregulated (Table S4).

3.3 BBR reshapes gut microbiota composition

We performed 16S rRNA sequencing to characterize gut microbiota profiles in the Ctrl, PBC, and BBR groups. α-diversity analysis revealed that the BBR group exhibited significantly lower Sobs, Chao, and Shannon indices than both the Ctrl and PBC groups (Fig. 3A). Principal coordinates analysis

demonstrated distinct clustering among the three groups, with the BBR group forming an independent cluster (Fig. 3B). Differences in relative microbial abundance among groups were further explored using LEfSe analysis (Fig. S1-4).

At the family level, PBC mice showed a marked reduction in Muribaculaceae, Atopobiaceae, Erysipelotrichaceae, and Bifidobacteriaceae compared with the Ctrl group. BBR treatment partially restored the abundance of these taxa, significantly reduced the relative abundance of Rikenellaceae, Tannerellaceae, and Enterobacteriaceae, and increased the relative abundance of Akkermansiaceae (Fig. 3C). Muribaculaceae, Erysipelotrichaceae, Bifidobacteriaceae, and Atopobiaceae showed predominantly positive correlations with genes involved in bile secretion genes. In contrast, Rikenellaceae, Tannerellaceae, and Enterobacteriaceae showed negative correlations (Fig. 3D).

At the genus level, PBC mice exhibited increased abundances of *Bacteroides* and *Parabacteroides*, along with decreased levels of *Dubosiella*, *Lactobacillus*, *Bifidobacterium*, and unclassified members of Muribaculaceae (norank_f__Muribaculaceae). These alterations were largely reversed by BBR treatment, which also significantly enriched *Akkermansia* and reduced the abundance of *Alistipes* (Fig. 3E). *Lactobacillus*, *Bifidobacterium*, *Dubosiella*, and *norank_f__Muribaculaceae* were positively associated with bile secretion genes, whereas *Bacteroides*, *Parabacteroides*, and *Alistipes* showed negative correlations (Fig. 3F).

3.4 Establishment and characterization of human bile–derived cholangiocyte organoids

As shown in Fig. 4A, partial cells began to form early organoid structures with vacuole-like morphology one day after seeding. During days 4–5 of culture, the organoids rapidly increased in size. By day 7, typical cholangiocyte organoids with diameters ranging from 50 to 200 μm were clearly observed under light microscopy, exhibiting well-defined boundaries, uniform refractivity, and a bright cystic appearance. The first passage was performed on day 10, after which the growth rate of first-passage (P1) organoids was slightly slower than that of primary organoids. Following a second passage, P2 organoids cultured for 5 days were stained with H&E. Histological analysis revealed that the organoids consisted of a single layer of regularly arranged epithelial cells surrounding a distinct central lumen (Fig. 4B).

To identify the cellular identity of the organoids, immunofluorescence staining was performed for the cholangiocyte marker CK19 and the hepatocyte marker albumin (ALB). As shown in Fig. 4C, CK19 was positively expressed in a ring-like pattern surrounding the luminal structure, whereas ALB expression was not detected, indicating the absence of hepatocytic characteristics. Furthermore, co-immunostaining for the epithelial cell adhesion molecule epithelial cell adhesion molecule (EpCAM) and the cholangiocyte-specific transcription factor SRY-box transcription factor 9 (Sox9) demonstrated positive expression of both markers. EpCAM signals were localized to the cell membrane, while Sox9 signals were predominantly distributed around the nucleus, forming a characteristic cholangiocyte epithelial signature (Fig. 4D). Collectively, these results confirm that the established organoids possess definitive cholangiocyte epithelial identity.

3.5 BBR mitigates H_2O_2–induced morphological deterioration, cell death, and senescence in cholangiocyte organoids

In PBC, oxidative stress injury is also a important mechanism contributing to biliary epithelial cell damage. To address how BBR protects biliary epithelial cells from oxidative stress injury, we employed an in vitro H_2O_2-induced injury model in human bile-derived cholangiocyte organoids.

Cholangiocyte organoids exposed to 2.5 μM H_2O_2 exhibited pronounced morphological deterioration, characterized by marked shrinkage, irregular and rough edges, and the presence of dark areas and granular structures compared with the Ctrl group. Notably, BBR intervention significantly ameliorated H_2O_2-induced morphological alterations, displaying a more intact, compact, and spherical architecture (Fig. 5A). Figure 5B presents the corresponding H&E staining results. Immunofluorescence analysis showed that, compared with the Ctrl group, P21 fluorescence intensity was markedly increased in the H_2O_2 group, whereas BBR treatment significantly reduced P21 expression (Fig. 5C).

SA-β-gal staining revealed intense blue staining in the H_2O_2 group, whereas staining intensity was markedly reduced in the BBR group, indicating that BBR alleviated cellular senescence (Fig. 5D). AO/PI staining demonstrated that the Ctrl group was predominantly composed of viable cells exhibiting green fluorescence, with only a few dead cells showing red fluorescence. In contrast, the H_2O_2 group was dominated by red fluorescent dead cells, with extensive accumulation of dead cells within organoids and scattered dead cells in the background. In the BBR group, viable and dead cells coexisted at a relatively balanced proportion, and the overall cellular condition was markedly improved compared with the H_2O_2 group (Fig. 5E). Maximum intensity projection images further showed that organoids in the H_2O_2 group exhibited reduced fluorescence intensity, pronounced shrinkage, and decreased size, whereas BBR-treated organoids displayed stronger fluorescence signals, more intact morphology, larger cell size, and well-preserved structural integrity (Fig. 5F).

3.6 BBR preserves ultrastructure and suppresses oxidative stress–triggered inflammatory responses in cholangiocyte organoids

TEM revealed distinct differences in mitochondrial ultrastructure among the three groups. In the Ctrl group, cells exhibited intact ultrastructural organization with microvilli extending into the lumen, tight intercellular junctions, and mitochondria displaying clear double membranes with densely and orderly arranged cristae, without apparent pathological alterations. In contrast, cells in the H_2O_2 group showed markedly loosened intercellular junctions, atrophied microvilli, and severe mitochondrial damage, characterized by mitochondrial swelling, disruption of membrane integrity, fragmentation or loss of cristae, and vacuolar degeneration, indicative of oxidative stress–induced mitochondrial dysfunction. Following BBR intervention, cellular ultrastructure was substantially improved, with relatively intact cell

membranes, partial restoration of intercellular junctions, and attenuation of mitochondrial swelling, accompanied by partial recovery of mitochondrial membranes and cristae structures (Fig. 7A).

RT-qPCR analysis further showed that mRNA levels of CX3CL1, CXCL10, CXCL2, and IL-8 were significantly elevated in organoids following oxidative stress induction, while BBR intervention significantly downregulated the expression of CX3CL1, CXCL10, and IL-8 (Fig. 7B). Consistently, ELISA of organoid culture supernatants revealed that BBR significantly reduced the secretion levels of pro-inflammatory cytokines, including CXCL2, TNF-α, CXCL10, and IL-8 (Fig. 7C).

3.7 BBR restores metabolic transcriptional programs in cholangiocyte organoids

Organoid transcriptome analysis showed that showing clear separation among the Ctrl, H_2O_2, and BBR groups (Fig. 7A). Compared to the H_2O_2 group, BBR intervention significantly upregulated 18 genes and downregulated 8 genes (Fig. 7B-C). KEGG enrichment analysis showed BBR intervention led to the upregulation of metabolic pathways, alongside the downregulation of pathways associated with inflammation and injury, such as the mitogen-activated protein kinase (MAPK) signaling pathway and the complement and coagulation cascades. (Fig. 7D). GSEA further confirmed that BBR upregulated glycolysis/gluconeogenesis, fructose and mannose metabolism, and ribosome-related pathways, while downregulating DNA damage–associated carcinogenic pathways (Fig. 7E).

3.8 BBR attenuates inflammation and cell death–related proteomic changes in cholangiocyte organoids

Olink proteomic profiling demonstrated clear separation among the Ctrl, H_2O_2, and BBR groups, as evidenced by PCA and differential protein expression analysis (Fig. 8A). Compared to the H_2O_2 group, BBR intervention significantly upregulated 34 proteins and downregulated 201 proteins (Fig. S5). Notably, CHRM3, CCL28, and HRC were significantly upregulated, while HIF1A, NFKB1, and NFKBIE were markedly downregulated following BBR intervention (Fig. 8B-C).

KEGG enrichment analysis showed that, compared with the H_2O_2 group, differentially expressed proteins in the BBR group were significantly enriched in TNF, NF-κB signaling pathways, and apoptosis, with additional enrichment in autophagy and mitophagy pathways. GO enrichment analysis further revealed involvement in apoptosis and NF-κB signaling transduction (Fig. 8D-E). Protein–protein interaction network analysis revealed that HIF1A exhibited the highest degree of connectivity, followed by BCL2L1 and NFKB1, and showed strong interactions with both proteins (Fig. 8F). GSEA further demonstrated that BBR intervention positively enriched pathways related to mucin-type O-glycosylation, keratan sulfate glycosaminoglycan biosynthesis, and peroxisome-associated functions, while pathways associated with Toll-like receptor signaling, RIG-I–like receptor signaling, and apoptosis were significantly negatively enriched (Fig. 8G).

4. Discussion

While BBR has demonstrated protective effects in PSC and cholestatic hepatitis(Kowdley et al., 2022; Tu et al., 2025; Wang et al., 2024), its efficacy and mechanisms in PBC remain unclear. Our study reveals a dual-pronged mechanism for BBR in PBC: it restores intestinal homeostasis to remodel liver metabolism and directly protects biliary epithelial cells from oxidative stress-induced injury. These findings establish BBR's protective role and provide novel mechanistic insights, positioning it as a potential therapeutic candidate for PBC.

Gut microbiota has been identified in multiple studies as an essential mechanism underlying the effectiveness of BBR (Habtemariam, 2020; Tian et al., 2019). For instance, BBR has been demonstrated to modulate tryptophan metabolism-related metabolites that activate the aryl hydrocarbon receptor thereby improving colitis (Jing et al., 2020). Additionally, BBR increases the activity of key enzymes involved in short-chain fatty acid (SCFA) production, as well as the abundance of SCFA-producing bacteria, such as *Akkermansia*, which not only helps regulate metabolic homeostasis but also enhances intestinal barrier function, reducing lipopolysaccharide (LPS) translocation into the bloodstream and inhibiting inflammatory pathways (Cheng et al., 2021; Wang et al., 2017). Moreover, previous studies have shown that BBR reduces the abundance of potential pathogenic bacteria while increasing beneficial microbes, such as *Bifidobacterium adolescentis* and *Lactobacillus acidophilus*, and enhance the Bacteroidetes-to-Firmicutes ratio in obese animals (Habtemariam, 2020). In patients with PBC, the abundance of beneficial bacteria decreases, while harmful bacteria such as *Enterobacteriaceae*, *Streptococcus*, and *Klebsiella* increase (Lv et al., 2016). BBR has shown antibacterial activity against *Streptococcus* and *Klebsiella* (Du et al., 2020; Zhou et al., 2016), suggesting its potential in improving the microbial imbalance observed in PBC.

Consistently, BBR treatment in PBC mice led to a reduction in gut microbial α-diversity; however, the overall microbial community structure was favorably reshaped. Specifically, beneficial genera such as *Lactobacillus* and *Bifidobacterium* were restored or enriched, while potentially pathogenic taxa, including members of the *Enterobacteriaceae* family, were markedly reduced. *Muribaculaceae*, a dominant bacterial family in the feces of C57BL/6J mice (Ormerod et al., 2016), is known to engage in cross-feeding interactions with probiotics such as bifidobacteria and lactobacilli and to produce short-chain fatty acids. Its abundance has been positively associated with the alleviation of inflammatory bowel disease, obesity, and type 2 diabetes (Zhu et al., 2024). In this study, *Muribaculaceae* exhibited the highest relative abundance under physiological conditions but was significantly reduced in PBC mice, partially restored following BBR treatment, and positively correlated with multiple bile acid metabolism–related genes. Nevertheless, its precise role in PBC pathophysiology warrants further investigation. Jiang et al. demonstrated that PBC mice receiving FMT from PBC patients developed more severe liver injury than those receiving FMT from healthy donors, with significant enrichment of *Alistipes* and *Bacteroides*(Jiang et al., 2024), findings highly consistent with the gut microbial features observed in our PBC model. Notably, BBR markedly reduced the relative abundance of these taxa. In addition, BBR treatment significantly increased the abundance of *Akkermansia*, which has been demonstrated to improve intestinal barrier function and reduce plasma LPS levels (Cani et al., 2022), promote bile acid synthesis and excretion–related gene expression in models of metabolic dysfunction–associated fatty liver

disease (Rao et al., 2021), and synergize with Bifidobacterium bifidum to activate hepatic FXR signaling in nonalcoholic fatty liver disease models (Nian et al., 2023). Importantly, the therapeutic effects of BBR on Akkermansia abundance appear to be time- and dose-dependent (Dong et al., 2021). Collectively, these findings suggest that gut microbiota remodeling may contribute to the amelioration of PBC progression, though the mechanisms are yet to be fully understood.

In vivo experiments demonstrated that BBR restored key metabolic pathways, including oxidative phosphorylation and bile secretion, while downregulating chemokine signaling and NF-κB signaling pathways, thereby improving liver function and attenuating fibrosis. In cholangiocyte organoids, BBR significantly reduced the expression of NF-κB–related proteins, including NFKB1 and NFKBIE, and decreased the levels of pro-inflammatory cytokines such as TNF-α, ultimately alleviating apoptosis. Accumulation of hydrophobic bile acids within cholangiocytes has been implicated in bile duct injury and inflammatory responses in PBC patients (Reshetnyak & Maev, 2023), and in the acceleration of liver fibrosis in PBC mouse models(Yamashita et al., 2023). Unlike humans, in whom bile acid detoxification is primarily mediated by 3α-hydroxyl sulfation via SULT2A1, mice rely predominantly on 7-hydroxyl sulfation catalyzed by Sult2a8(Wang et al., 2021). In this study, BBR significantly upregulated hepatic Sult2a8 expression in PBC mice, thereby reducing bile acid toxicity. Consistent with our findings, previous studies in Mdr2$^{-/-}$ genetic cholestasis and 3,5-Diethoxycarbonyl-1,4-dihydrocollidine (DDC) -induced models demonstrated that BBR upregulated multiple bile acid metabolism–related genes, including Cyp7a1, Shp, Fxr, and Bsep, maintained bile acid homeostasis, suppressed NF-κB signaling, and markedly improved liver fibrosis and ductular reaction(Hameed et al., 2024; Wang et al., 2024). Moreover, a recent clinical trial reported that an ionic salt formulation of BBR combined with UDCA (HTD1801) significantly reduced alkaline phosphatase levels in patients with primary sclerosing cholangitis and exhibited a favorable safety profile(Kowdley et al., 2022).

Impairment of the biliary bicarbonate umbrella, characterized by insufficient HCO_3^- secretion, exacerbates bile duct injury in PBC (Reshetnyak & Maev, 2023). In this study, BBR treatment significantly increased the expression of CHRM3 (muscarinic acetylcholine receptor 3, mAChR3) and HRC proteins in cholangiocyte organoids and upregulated mucin barrier–associated proteins. CHRM3 activates Ca^{2+}-dependent secretory processes via the Gq–IP_3–Ca^{2+} signaling cascade, thereby stimulating bicarbonate secretion mediated by the Cl^-/HCO_3^- anion exchanger 2(Boyer, 2013). Previous studies have shown that M3 receptor–deficient mice are more susceptible to DDC-induced cholestatic liver injury (Durchschein et al., 2017), and inhibitory autoantibodies against mAChR3 have been detected in PBC patients (Mayer et al., 2020). In addition, HRC, an endoplasmic reticulum luminal Ca^{2+}-binding protein, contributes to the maintenance of intracellular Ca^{2+} homeostasis (Arvanitis et al., 2010). These findings suggest that BBR may restore cholangiocyte secretory function and epithelial homeostasis by enhancing CHRM3-mediated Ca^{2+}-dependent Cl^-/HCO_3^- exchange and stabilizing HRC-associated Ca^{2+} signaling.

Chronic inflammatory microenvironments resulting from immune intolerance, bile acid toxicity, and dysfunction of the bicarbonate umbrella synergistically enhance oxidative stress in cholangiocytes, increasing intracellular reactive oxygen species (ROS) levels and subsequent cellular dysfunction and

injury. In vivo, BBR exerted significant protective effects by upregulating PPAR signaling and glutathione metabolism pathways in PBC mice. In vitro, BBR similarly enhanced the expression of peroxisome-related proteins under H_2O_2–induced oxidative stress, promoted metabolic adaptation, upregulated genes associated with mitochondrial function, and markedly restored mitochondrial morphology and intercellular junction integrity. Previous studies have demonstrated that BBR exerts antioxidant effects by enhancing endogenous antioxidant enzyme activity and activating Nrf2 and MAPK signaling pathways (García-Muñoz et al., 2024). PPARs, as key members of the nuclear hormone receptor family, play essential roles in lipid metabolism, energy homeostasis, inflammation, and oxidative stress, and are critically involved in the improvement of cholestatic liver injury(Changizi et al., 2023). As a natural ligand of PPARs, BBR effectively activates PPAR-α and PPAR-δ, thereby participating in key anti-inflammatory and antioxidant regulatory processes(Owumi et al., 2024; Yu et al., 2016). In this study, BBR predominantly activated PPAR-α, which is highly expressed in the liver. Activation of PPAR-α not only upregulates multiple antioxidant genes but also suppresses inflammatory signaling pathways such as NF-κB (Singh & Chaudhary, 2025). Consequently, BBR may inhibit hepatic stellate cell activation by reducing oxidative stress and pro-inflammatory cytokine levels and activating nuclear receptor–mediated pathways, thereby attenuating liver fibrosis. Notably, previous studies have also shown that BBR can induce ferrous iron redox reactions and activate ROS-mediated ferroptosis in hepatic stellate cells, further contributing to the alleviation of liver fibrosis(Chen et al., 2024; Feng et al., 2025; Yi et al., 2021).

Several limitations of this study should be acknowledged. First, the investigation primarily relied on a chemically-induced murine model of PBC and an in vitro H_2O_2-induced injury model using cholangiocyte organoids. Although widely utilized, these models do not fully recapitulate the complex pathogenesis of human PBC. Future studies are needed to validate the therapeutic efficacy of BBR in more diverse model systems and ultimately in human cohorts. Second, while we observed that BBR modulated the gut microbiota and improved liver injury concurrently, this association remains largely correlative. Further studies employing interventions such as fecal microbiota transplantation (FMT) or germ-free animal models are warranted to establish direct causal evidence for the role of the microbiome in mediating the beneficial effects of BBR. Finally, although our work has preliminarily mapped the molecular landscape associated with BBR's action, subsequent in-depth molecular and pharmacological experiments are necessary to dissect and validate the hierarchy and functional necessity of the identified pathways.

5. Conclusion

In conclusion, this study demonstrates that BBR exerts significant hepatoprotective effects in PBC. These benefits are mechanistically linked to a dual mode of action: systemically, BBR reshapes gut microbiota and activates hepatic protective pathways, including PPAR signaling and glutathione metabolism; locally, it directly mitigates oxidative stress-induced injury in biliary epithelial cells by restoring mitochondrial function and suppressing pro-inflammatory signaling. Collectively, our findings position BBR as a promising multi-target therapeutic candidate for PBC, acting through the gut-liver axis and directly on cholangiocyte pathophysiology. Future studies focusing on the validation of these

identified core targets and early-phase clinical trials will be crucial to translate these promising preclinical findings into therapeutic applications.

Abbreviations

2-OA-BSA
2-Octynoic Acid–Bovine Serum Albumin
ALT
Alanine Aminotransferase
AST
Aspartate Aminotransferase
BBR
Berberine Hydrochloride
CK19
Cytokeratin 19
CXCL
C-X-C Motif Chemokine Ligand
FMT
Fecal Microbiota Transplantation
FXR
Farnesoid X Receptor
GGT
Gamma-Glutamyl Transferase
IL
Interleukin
LPS
lipopolysaccharide
NF-κB
Nuclear Factor Kappa-B
PBC
Primary Biliary Cholangitis
PPAR
Peroxisome Proliferator-Activated Receptor
PSC
Primary Sclerosing Cholangitis
TNF
Tumor Necrosis Factor
UDCA
Ursodeoxycholic Acid.

Declarations

Declaration of competing interest

The authors declare that they have no known competing financial interests or personal relationships that could have appeared to influence the work reported in this paper.

Ethics approval and consent to participate

This study was approved by the Clinical Research Ethics Committee of the First Affiliated Hospital, Zhejiang University School of Medicine. Human tissue–derived organoid experiments were approved under protocol number IIT20220456B–R1 (title of the project: Innovative pathogenesis of autoimmune diseases in the elderly and establishment of diagnosis and treatment/intervention strategies; name of the institutional approval committee: Clinical Research Ethics Committee of the First Affiliated Hospital, College of Medicine, Zhejiang University; the approval number: IIT20220456B–R1; date of approval: 15 Nov 2022). All animal experiments were approved under protocol number 2026–004 (title of the project: Mechanism research of berberine regulating gut-liver axis to alleviate primary biliary cholangitis in mouse models; name of the institutional approval committee: Animal Experimental Ethics Committee of The First Affiliated Hospital, Zhejiang University School of Medicine; the approval number: 2026–004; date of approval: 05 January 2026). The patients provided written informed consent for participation in the study and the use of bile samples.

Author Contribution

Yechen Wu and Yuxi Zhao: Conceptualization, Data curation, Writing – original draft, Methodology. Kaicen Wang: Conceptualization, Project administration. Tinglei Song, Yulan Pan, and Qianhan Xie: Formal analysis. Pengyu Yin, Fengjiao Wang, and Jiali Ni: Data curation. Andreas.teufel:Writing-review editing,Yanfei Chen and Lanjuan Li: Conceptualization, Funding acquisition, Supervision.

Acknowledgement

This work was supported by Key R&D Program of Shandong Province, China (No: 2025CXPT013); Research Project of Jinan Microecological Biomedicine Shangdong Laboratory (No. JNL-2025001A); National Key R&D Program of China (2022YFC3602000), and Natural Science Foundation of China 32270068.

References

1. Arvanitis DA, Vafiadaki E, Sanoudou D, Kranias EG. Histidine-rich calcium binding protein: the new regulator of sarcoplasmic reticulum calcium cycling. J Mol Cell Cardiol. 2010;50(1):43–9. https://doi.org/10.1016/j.yjmcc.2010.08.021.
2. Boyer JL. Bile formation and secretion. Compr Physiol. 2013;3(3):1035–78. https://doi.org/10.1002/cphy.c120027.
3. Cani PD, Depommier C, Derrien M, Everard A, de Vos WM. Akkermansia muciniphila: paradigm for next-generation beneficial microorganisms. Nat Rev Gastroenterol Hepatol. 2022;19(10):625–37. https://doi.org/10.1038/s41575-022-00631-9.
4. Changizi Z, Kajbaf F, Moslehi A. An Overview of the Role of Peroxisome Proliferator-activated Receptors in Liver Diseases. J Clin Translational Hepatol. 2023;11(7):1542–52. https://doi.org/10.14218/JCTH.2023.00334.
5. Chen G, Zhang C, Zou J, Zhou Z, Zhang J, Yan Y, Feng Y. Coptidis rhizoma and berberine as anti-cancer drugs: A 10-year updates and future perspectives. Pharmacol Res. 2025;216:107742. https://doi.org/10.1016/j.phrs.2025.107742.
6. Chen W, Lin F, Feng X, Yao Q, Yu Y, Gao F, Yang JJA. J. o. P. S. (2024). MSC-derived exosomes attenuate hepatic fibrosis in primary sclerosing cholangitis through inhibition of Th17 differentiation. *19*(1), 100889.
7. Cheng H, Liu J, Tan Y, Feng W, Peng C. Interactions between gut microbiota and berberine, a necessary procedure to understand the mechanisms of berberine. J Pharm Anal. 2021;12(4):541–55. https://doi.org/10.1016/j.jpha.2021.10.003.
8. Dong C, Yu J, Yang Y, Zhang F, Su W, Fan Q, Wu S. Berberine, a potential prebiotic to indirectly promote Akkermansia growth through stimulating gut mucin secretion. Biomed Pharmacotherapy = Biomedecine Pharmacotherapie. 2021;139:111595. https://doi.org/10.1016/j.biopha.2021.111595.
9. Du G-F, Le Y-J, Sun X, Yang X-Y, He Q-Y. Proteomic investigation into the action mechanism of berberine against Streptococcus pyogenes. J Proteom. 2020;215:103666. https://doi.org/10.1016/j.jprot.2020.103666.
10. Durchschein F, Krones E, Pollheimer MJ, Zollner G, Wagner M, Raufman J-P, Fickert P. Genetic loss of the muscarinic M3 receptor markedly alters bile formation and cholestatic liver injury in mice. Hepatol Research: Official J Japan Soc Hepatol. 2017;48(3):E68–77. https://doi.org/10.1111/hepr.12928.
11. Feng X, Feng B, Zhou J, Yang J, Pan Q, Yu J, Cao HJH. (2025). Mesenchymal stem cells alleviate mouse liver fibrosis by inhibiting pathogenic function of intrahepatic B cells. *81*(4), 1211–27.
12. García-Muñoz AM, Victoria-Montesinos D, Ballester P, Cerdá B, Zafrilla P. A Descriptive Review of the Antioxidant Effects and Mechanisms of Action of Berberine and Silymarin. Molecules. 2024;29(19). https://doi.org/10.3390/molecules29194576.
13. Habtemariam S. Berberine pharmacology and the gut microbiota: A hidden therapeutic link. Pharmacol Res. 2020;155:104722. https://doi.org/10.1016/j.phrs.2020.104722.

14. Hameed H, Irshad N, Yousaf MA, Mumtaz S, Sohail I. Berberine ameliorates the progression of primary sclerosing cholangitis by activating farnesoid X receptor. Cell Biochem Biophys. 2024;82(2):767–76. https://doi.org/10.1007/s12013-024-01226-8.
15. Harms MH, Lammers WJ, Thorburn D, Corpechot C, Invernizzi P, Janssen HLA, van Buuren HR. Major Hepatic Complications in Ursodeoxycholic Acid-Treated Patients With Primary Biliary Cholangitis: Risk Factors and Time Trends in Incidence and Outcome. Am J Gastroenterol. 2018;113(2):254–64. https://doi.org/10.1038/ajg.2017.440.
16. Huang Y, He K, Chen YJIM, Diseases. (2023). Unraveling Interactions Between Gut Epithelium and Microbiota Using Models of Intestinal Organoids. 10.1097
17. Jiang H, Yu Y, Hu X, Du B, Shao Y, Wang F, Lv L. The fecal microbiota of patients with primary biliary cholangitis (PBC) causes PBC-like liver lesions in mice and exacerbates liver damage in a mouse model of PBC. Gut Microbes. 2024;16(1):2383353. https://doi.org/10.1080/19490976.2024.2383353.
18. Jing W, Dong S, Luo X, Liu J, Wei B, Du W, Lu H. Berberine improves colitis by triggering AhR activation by microbial tryptophan catabolites. Pharmacol Res. 2020;164:105358. https://doi.org/10.1016/j.phrs.2020.105358.
19. Komori A, Kugiyama Y. Hard-to-treat autoimmune hepatitis and primary biliary cholangitis: The dawn of a new era of pharmacological treatment. Clin Mol Hepatol. 2025;31(1). https://doi.org/10.3350/cmh.2024.0821.
20. Kowdley KV, Forman L, Eksteen B, Gunn N, Sundaram V, Landis C, Hirschfield GM. A Randomized, Dose-Finding, Proof-of-Concept Study of Berberine Ursodeoxycholate in Patients With Primary Sclerosing Cholangitis. Am J Gastroenterol. 2022;117(11):1805–15. https://doi.org/10.14309/ajg.0000000000001956.
21. Li Z, Wang Y, Xu Q, Ma J, Li X, Yan J, Chen T. Berberine and health outcomes: An umbrella review. Phytother Res. 2023;37(5):2051–66. https://doi.org/10.1002/ptr.7806.
22. Lindor KD, Bowlus CL, Boyer J, Levy C, Mayo M. Primary biliary cholangitis: 2021 practice guidance update from the American Association for the Study of Liver Diseases. Hepatology (Baltimore MD). 2022;75(4):1012–3. https://doi.org/10.1002/hep.32117.
23. Liu Q, Huang B, Zhou Y, Wei Y, Li Y, Li B, Tang R. (2025). Gut microbiome pattern impacts treatment response in primary biliary cholangitis. *Med (New York, N.Y.)*, *6*(1), 100504. https://doi.org/10.1016/j.medj.2024.08.003
24. Lv L-X, Fang D-Q, Shi D, Chen D-Y, Yan R, Zhu Y-X, Li L-J. Alterations and correlations of the gut microbiome, metabolism and immunity in patients with primary biliary cirrhosis. Environ Microbiol. 2016;18(7):2272–86. https://doi.org/10.1111/1462-2920.13401.
25. Mayer C, Preuss B, Grottenthaler J, Berg C, Klein R. Antibodies to the Muscarinic Acetylcholine Receptor M3 in Primary Biliary Cholangitis Inhibit Receptor Function on Cholangiocytes. Front Immunol. 2020;11:1151. https://doi.org/10.3389/fimmu.2020.01151.

26. Nian F, Wu L, Xia Q, Tian P, Ding C, Lu X. Akkermansia muciniphila and Bifidobacterium bifidum Prevent NAFLD by Regulating FXR Expression and Gut Microbiota. J Clin Translational Hepatol. 2023;11(4):763–76. https://doi.org/10.14218/JCTH.2022.00415.
27. Ormerod KL, Wood DLA, Lachner N, Gellatly SL, Daly JN, Parsons JD, Hugenholtz P. Genomic characterization of the uncultured Bacteroidales family S24-7 inhabiting the guts of homeothermic animals. Microbiome. 2016;4(1):36. https://doi.org/10.1186/s40168-016-0181-2.
28. Owumi S, Chimezie J, Otunla M, Oluwawibe B, Agbarogi H, Anifowose M, Owoeye O. Prepubertal Repeated Berberine Supplementation Enhances Cerebrocerebellar Functions by Modulating Neurochemical and Behavioural Changes in Wistar Rats. J Mol Neuroscience: MN. 2024;74(3):72. https://doi.org/10.1007/s12031-024-02250-2.
29. Rao Y, Kuang Z, Li C, Guo S, Xu Y, Zhao D, Lu Y. Gut Akkermansia muciniphila ameliorates metabolic dysfunction-associated fatty liver disease by regulating the metabolism of L-aspartate via gut-liver axis. Gut Microbes. 2021;13(1). https://doi.org/10.1080/19490976.2021.1927633.
30. Reshetnyak VI, Maev IV. New insights into the pathogenesis of primary biliary cholangitis asymptomatic stage. World J Gastroenterol. 2023;29(37):5292–304. https://doi.org/10.3748/wjg.v29.i37.5292.
31. Singh A, Chaudhary R. Potentials of peroxisome proliferator-activated receptor (PPAR) α, β/δ, and γ: An in-depth and comprehensive review of their molecular mechanisms, cellular Signalling, immune responses and therapeutic implications in multiple diseases. Int Immunopharmacol. 2025;155:114616. https://doi.org/10.1016/j.intimp.2025.114616.
32. Tanaka A, Leung PSC, Gershwin ME. Pathogen infections and primary biliary cholangitis. Clin Exp Immunol. 2019;195(1):25–34. https://doi.org/10.1111/cei.13198.
33. Tanaka A, Ma X, Takahashi A, Vierling JM. Primary biliary cholangitis. Lancet. 2024;404(10457):1053–66. https://doi.org/10.1016/S0140-6736(24)01303-5.
34. Tang R, Wei Y, Li Y, Chen W, Chen H, Wang Q, Ma X. Gut microbial profile is altered in primary biliary cholangitis and partially restored after UDCA therapy. Gut. 2018;67(3):534–41. https://doi.org/10.1136/gutjnl-2016-313332.
35. Tian Y, Cai J, Gui W, Nichols RG, Koo I, Zhang J, Patterson AD. Berberine Directly Affects the Gut Microbiota to Promote Intestinal Farnesoid X Receptor Activation. Drug Metab Dispos. 2019;47(2):86–93. https://doi.org/10.1124/dmd.118.083691.
36. Tu D, Lu C, Guo J, Chen Q, Li X, Wang Y, Yang S. Gut microbiota-mediated berberine metabolism ameliorates cholestatic liver disease by suppressing 5-HT production. Clin Mol Hepatol. 2025. https://doi.org/10.3350/cmh.2025.0577.
37. Wakabayashi K, Lian Z-X, Leung PSC, Moritoki Y, Tsuneyama K, Kurth MJ, Gershwin ME. Loss of tolerance in C57BL/6 mice to the autoantigen E2 subunit of pyruvate dehydrogenase by a xenobiotic with ensuing biliary ductular disease. Hepatology (Baltimore MD). 2008;48(2):531–40. https://doi.org/10.1002/hep.22390.

38. Wang K, Chan Y-C, So P-K, Liu X, Feng L, Cheung W-T, Au SW-N. Structure of mouse cytosolic sulfotransferase SULT2A8 provides insight into sulfonation of 7α-hydroxyl bile acids. J Lipid Res. 2021;62:100074. https://doi.org/10.1016/j.jlr.2021.100074.
39. Wang Y, Shou J-W, Li X-Y, Zhao Z-X, Fu J, He C-Y, Jiang J-D. Berberine-induced bioactive metabolites of the gut microbiota improve energy metabolism. Metab Clin Exp. 2017;70:72–84. https://doi.org/10.1016/j.metabol.2017.02.003.
40. Wang Y, Zhao D, Su L, Tai YL, Way GW, Zeng J, Zhou H. Therapeutic potential of berberine in attenuating cholestatic liver injury: insights from a PSC mouse model. Cell Biosci. 2024;14(1):14. https://doi.org/10.1186/s13578-024-01195-8.
41. Yamashita M, Honda A, Shimoyama S, Umemura M, Ohta K, Chida T, Kawata K. Breach of tolerance versus burden of bile acids: Resolving the conundrum in the immunopathogenesis and natural history of primary biliary cholangitis. J Autoimmun. 2023;136:103027. https://doi.org/10.1016/j.jaut.2023.103027.
42. Yang Y, Choi J, Chen Y, Invernizzi P, Yang G, Zhang W, Gershwin ME. E. coli and the etiology of human PBC: Antimitochondrial antibodies and spreading determinants. Hepatology (Baltimore MD). 2022;75(2):266–79. https://doi.org/10.1002/hep.32172.
43. Yao Q, Chen W, Yu Y, Gao F, Zhou J, Wu J, Yu JJR. (2023). Human placental mesenchymal stem cells relieve primary sclerosing cholangitis via upregulation of TGR5 in Mdr2−/− mice and human intrahepatic cholangiocyte organoid models. *6*, 0207.
44. Yi J, Wu S, Tan S, Qin Y, Wang X, Jiang J, Wu B. Berberine alleviates liver fibrosis through inducing ferrous redox to activate ROS-mediated hepatic stellate cells ferroptosis. Cell Death Discovery. 2021;7(1):374. https://doi.org/10.1038/s41420-021-00768-7.
45. Yu H, Li C, Yang J, Zhang T, Zhou Q. Berberine is a potent agonist of peroxisome proliferator activated receptor alpha. Front Bioscience (Landmark Edition). 2016;21(5):1052–60.
46. Zhang M, Li Q, Zhou C, Zhao Y, Li R, Zhang Y. Demethyleneberberine attenuates concanavalin A-induced autoimmune hepatitis in mice through inhibition of NF-κB and MAPK signaling. Int Immunopharmacol. 2020;80:106137. https://doi.org/10.1016/j.intimp.2019.106137.
47. Zheng Q, Li Y, Zhu W, Xu X, Luo B, Sheng G, Diseases. Dynamic Relatsh Between Hum Microbiota Host Factors. 2024;6(3):106–7.
48. Zhou X-Y, Ye X-G, He L-T, Zhang S-R, Wang R-L, Zhou J, He Z-S. In vitro characterization and inhibition of the interaction between ciprofloxacin and berberine against multidrug-resistant Klebsiella pneumoniae. J Antibiot. 2016;69(10):741–6. https://doi.org/10.1038/ja.2016.15.
49. Zhu Y, Chen B, Zhang X, Akbar MT, Wu T, Zhang Y, Shen Q. Exploration of the Muribaculaceae Family in the Gut Microbiota: Diversity, Metabolism, and Function. Nutrients. 2024;16(16). https://doi.org/10.3390/nu16162660.

Figures

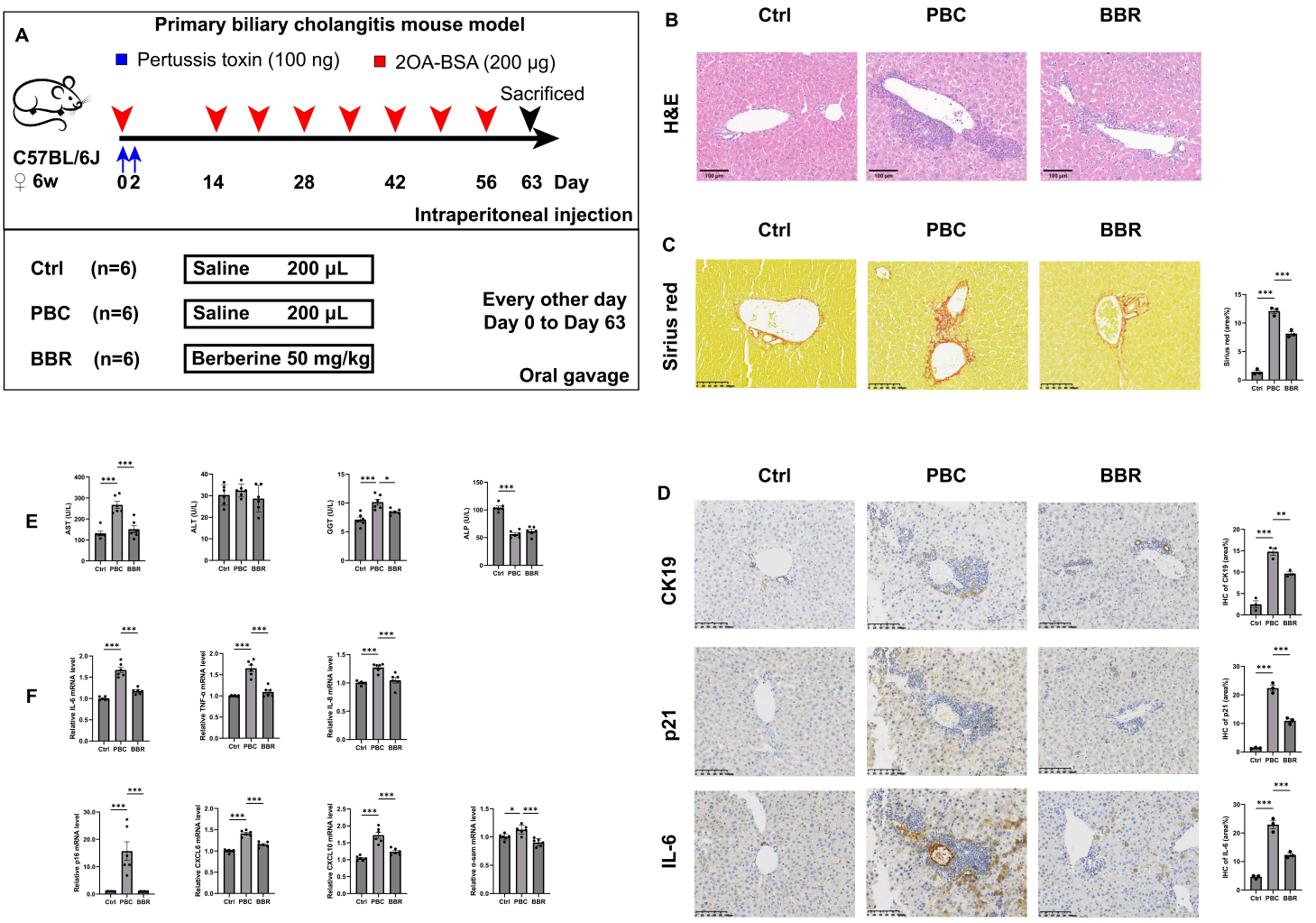


Figure 1

Berberine ameliorates liver injury, fibrosis and inflammation in a murine model of PBC

(A) Experimental scheme. (B) Representative H&E-stained liver sections showing that BBR alleviates portal inflammation. (C) Representative Sirius Red–stained liver sections with quantification of Sirius Red–positive area, showing that BBR reduces collagen deposition. (D) Representative IHC staining for CK19, p21, and IL-6, with corresponding quantification of positive staining areas, showing that BBR attenuates ductular reaction, cellular senescence, and inflammation. (E) Serum biochemical analysis of AST, ALT, ALP, and GGT, showing that BBR improves AST and GGT levels. (F) BBR reduces hepatic mRNA expression of α-SMA, CXCL6, CXCL10, IL-6, IL-8, p16, and TNF-α. *p < 0.05, **p < 0.01, ***p < 0.001.

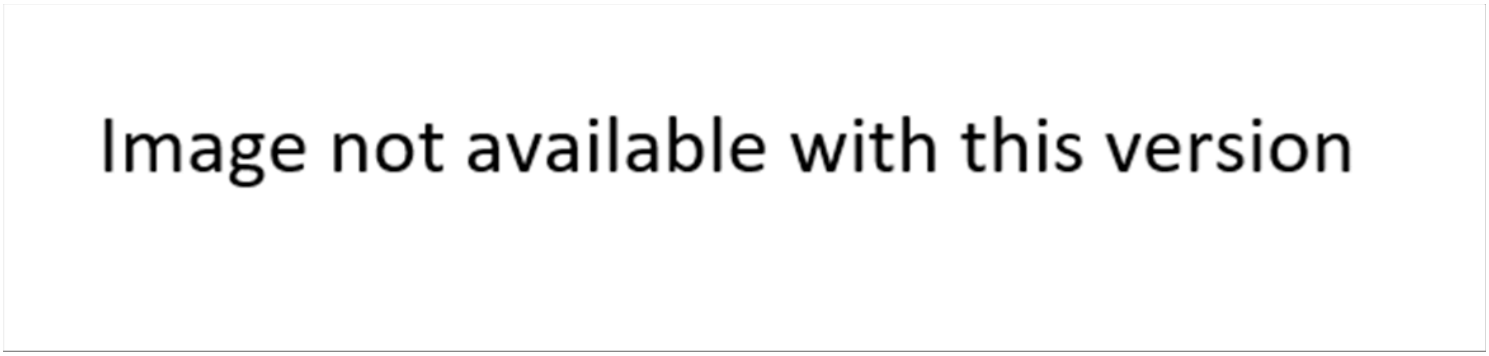


Figure 2

BBR restores metabolic pathways and suppresses inflammatory signaling in PBC livers

(A) PCA of liver transcriptomes showing clear separation among the Ctrl, PBC, and BBR groups. (B) Summary of differentially expressed genes (DEGs) (FC>2) for the indicated comparisons. (C) Volcano plot of DEGs in BBR vs. PBC. (D) KEGG pathway enrichment analysis of DEGs, highlighting the top upregulated and downregulated pathways in BBR vs. PBC. (E) GSEA showing bile secretion, oxidative phosphorylation, PPAR signaling, and glutathione metabolism pathways upregulated, and extracellular trap formation and complement and coagulation cascades pathways downregulated by BBR.

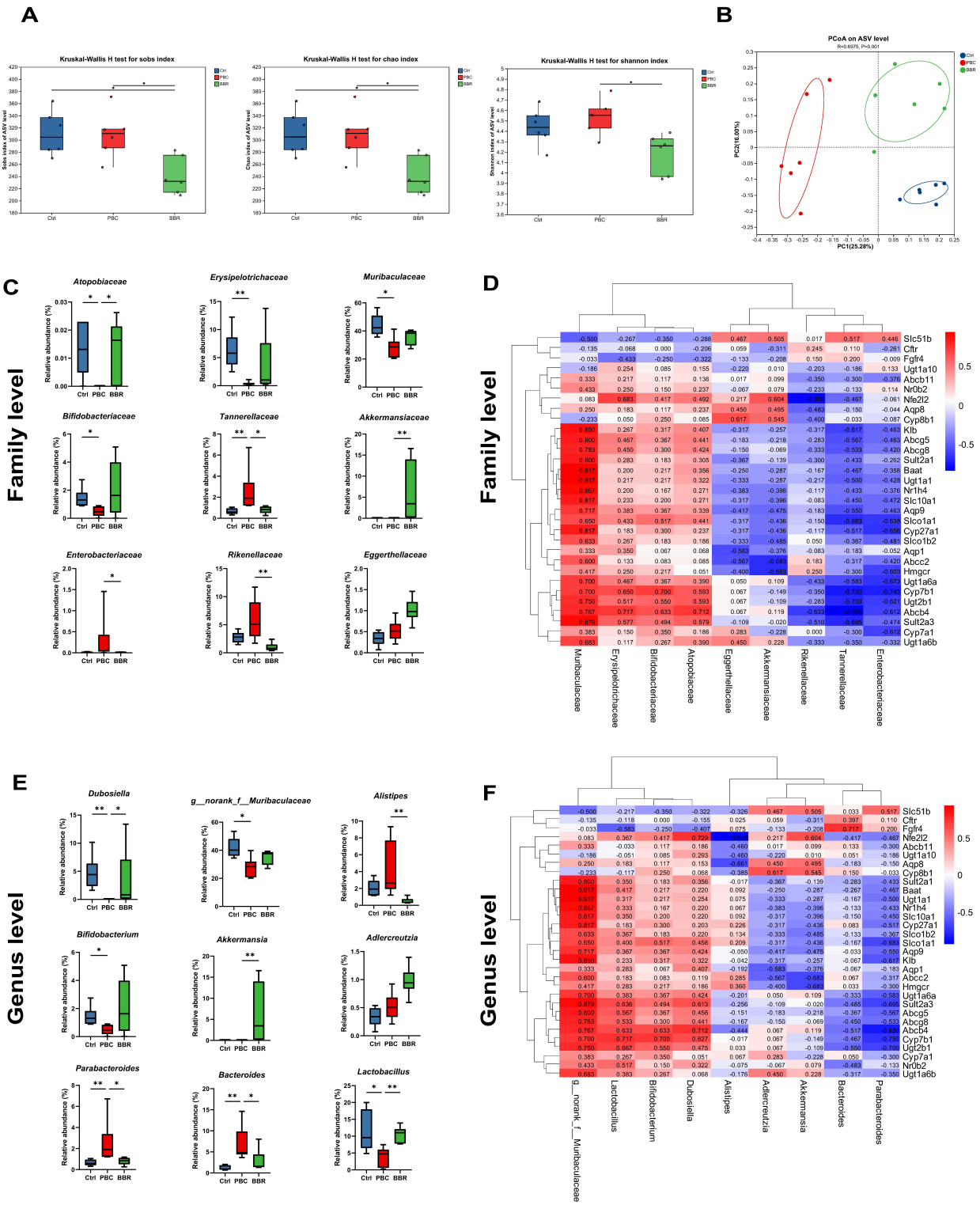


Figure 3

BBR reshapes gut microbiota composition

(A) Alpha diversity indices (Observed species, Shannon, Chao1) of gut microbiota showing BBR decrease Alpha diversity. (B) Principal coordinates analysis showing distinct community structures among groups. (C) Relative abundance of key bacterial families altered in PBC and partially restored by BBR. (D)

Correlation heatmap between bacterial families and hepatic bile secretion–related genes. (E) Relative abundance of key genera altered in PBC and partially restored by BBR. (F) Correlation heatmap between bacterial genera and hepatic bile secretion–related genes. *p < 0.05, **p < 0.01, ***p < 0.001.

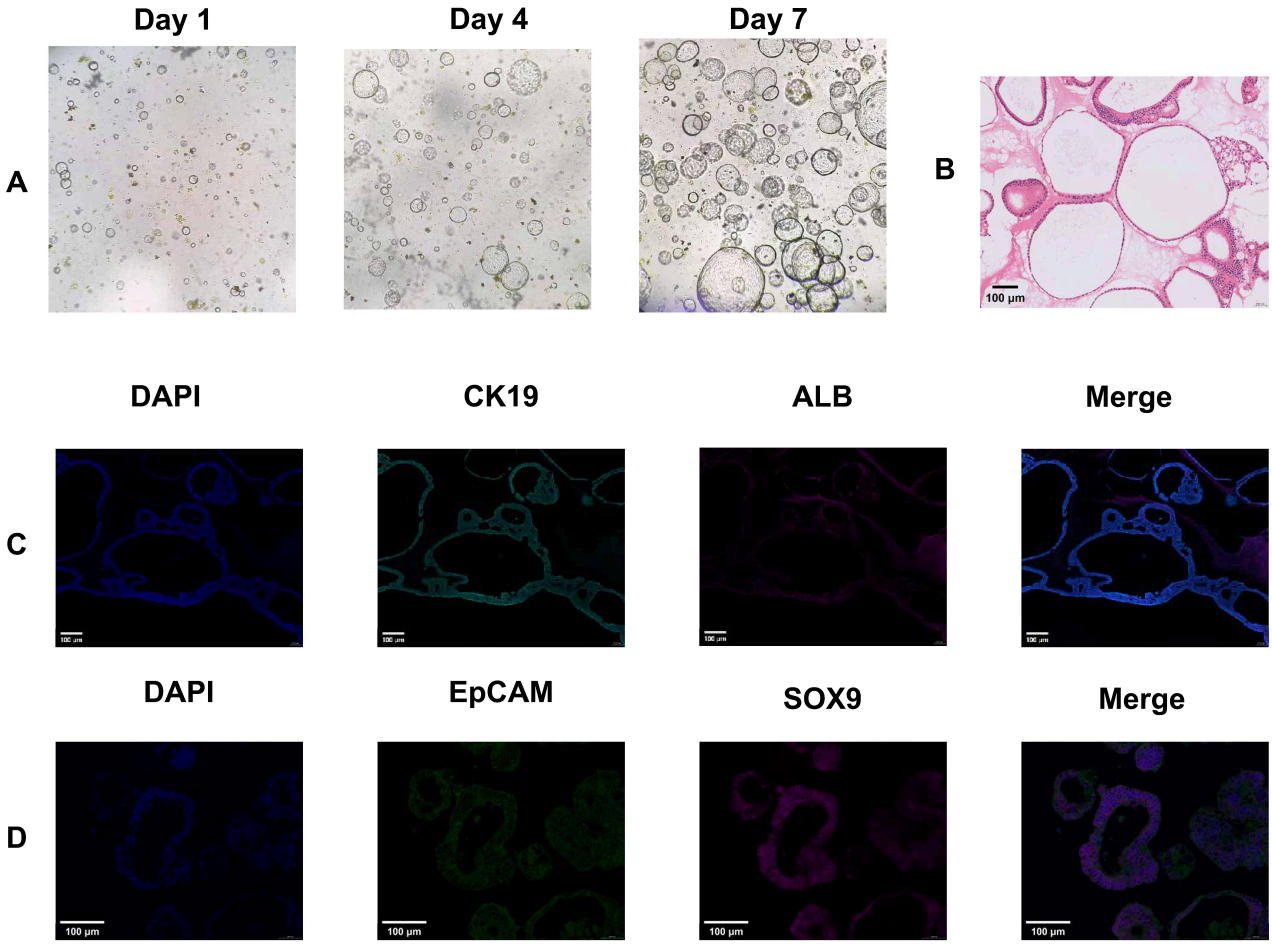


Figure 4

Establishment and characterization of human bile–derived cholangiocyte organoids

(A) Representative bright-field images showing organoid morphogenesis at days 1, 4, and 7 after seeding. (B) H&E staining of second-passage organoids showing a single epithelial layer surrounding a central lumen. (C) Immunofluorescence staining showing CK19-positive cholangiocyte identity and absence of hepatocyte marker ALB. (D) Co-immunofluorescence staining of EpCAM and SOX9 confirming cholangiocyte epithelial signature.

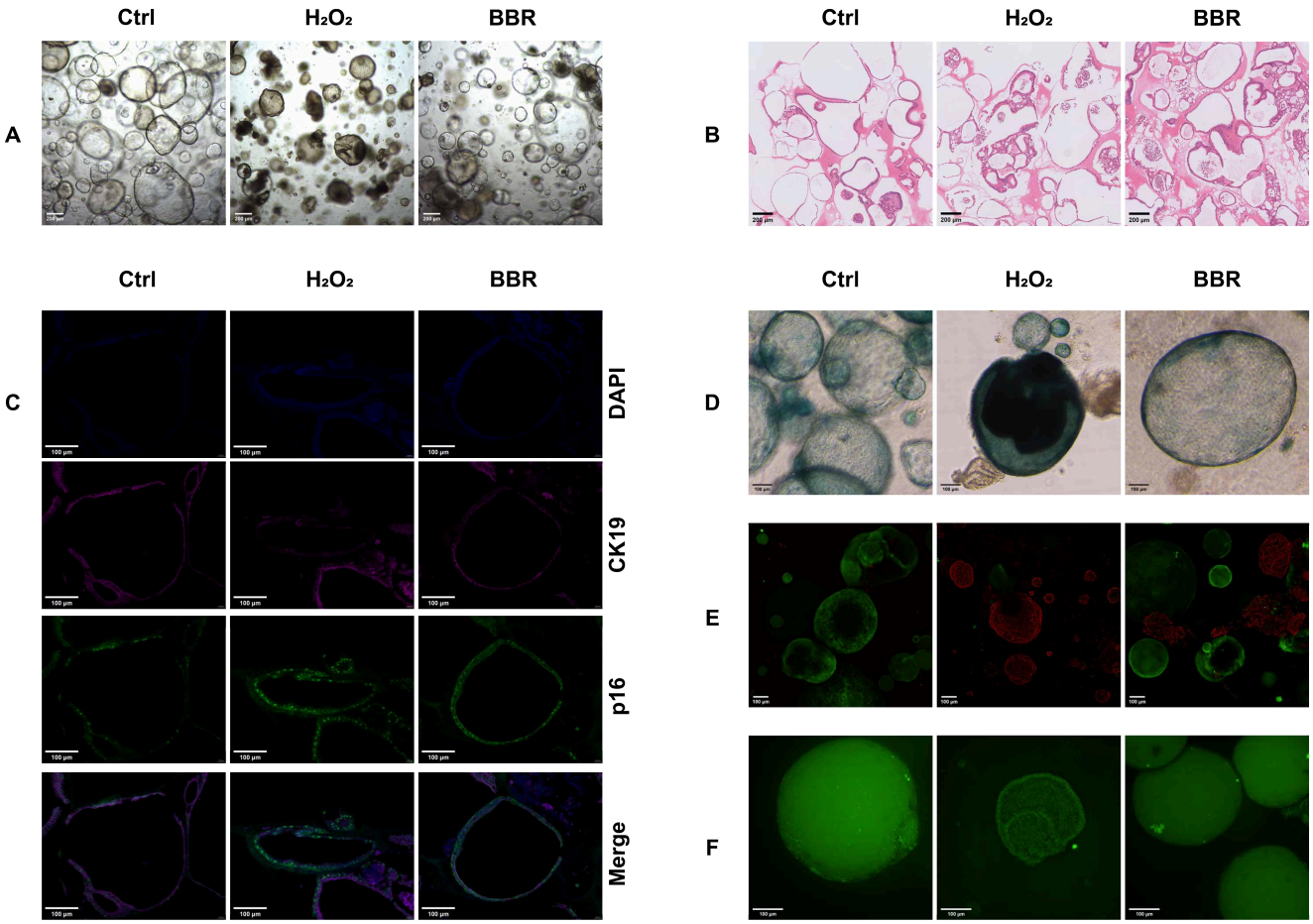


Figure 5

BBR mitigates H_2O_2–induced morphological deterioration, cell death, and senescence in cholangiocyte organoids

Cholangiocyte organoids (P2) were assigned to Ctrl, H_2O_2, and BBR groups; organoid morphology was monitored during a 7-day intervention. (A) Bright-field images showing H_2O_2-induced shrinkage and partial rescue by BBR. (B) H&E staining of organoids. (C) Immunofluorescence staining of p21 showing oxidative stress–induced senescence marker upregulation and reduction by BBR. (D) SA-β-gal staining showing that BBR reduces H_2O_2-induced cellular senescence in organoids. (E) AO/PI staining showing that BBR decreases H_2O_2-induced cell death (PI-positive, red). (F) Maximum intensity projection images showing that BBR maintains organoid structural integrity under H_2O_2 stress.

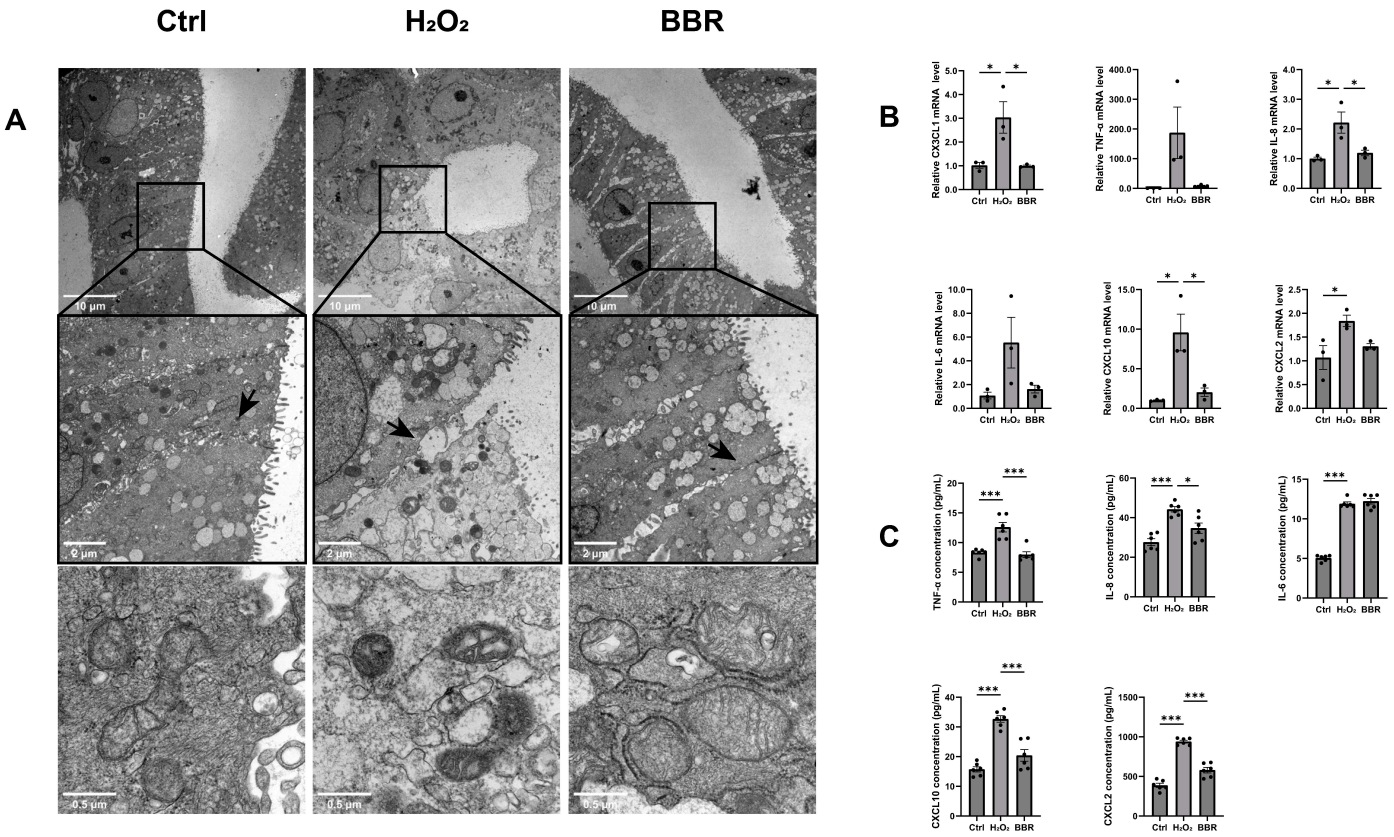


Figure 6

BBR preserves ultrastructure and suppresses oxidative stress–triggered inflammatory responses in cholangiocyte organoids

(A) TEM images showing microvilli, intercellular junction disrupted (arrows) and mitochondrial damaged under oxidative stress , and partial restoration by BBR. (B) Relative mRNAs expression levels of CX3CL1, CXCL10, CXCL2, IL-8 in organoids. (C) ELISA quantification of secreted cytokines and chemokines (TNF-α, CXCL2, CXCL10, IL-8) in culture supernatants. *P < 0.05, **P < 0.01, ***P < 0.001.

Image not available with this version

Figure 7

BBR restores metabolic transcriptional programs in cholangiocyte organoids

(A) PCA of organoid transcriptomes showing clear separation among the Ctrl, H_2O_2, and BBR groups. (B) Summary of DEGs (FC>2) for the indicated comparisons. (C) Volcano plot of DEGs in BBR vs. H_2O_2. (D) KEGG pathway enrichment analysis of DEGs, highlighting the top upregulated and downregulated pathways in BBR vs. H_2O_2. (E) GSEA showing ribosome, glycolysis/gluconeogenesis and fructose and mannose metabolism pathways upregulated, and chemical carcinogenesis-DNA adducts downregulated by BBR.

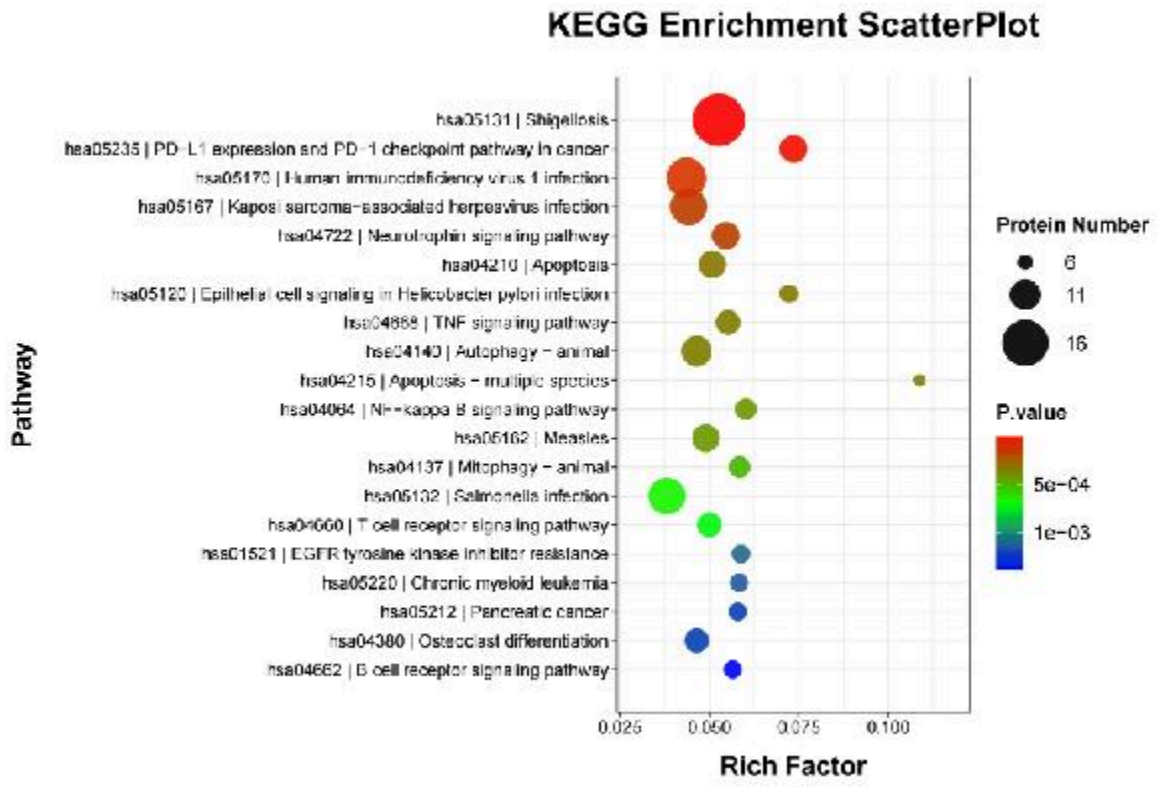


Figure 8

BBR attenuates inflammation and cell death–related proteomic changes in cholangiocyte organoids

(A) PCA of Olink-based proteomic profiles showing group separation among Ctrl, H_2O_2, and BBR. (B) Volcano plot of differentially expressed proteins (DEPs) in BBR vs H_2O_2. (C) Heatmap showing mean-centered abundance of representative DEPs in BBR vs H_2O_2. (D) KEGG pathway enrichment analysis of DEPs highlighting inflammatory signaling (TNF/NF-κB) and cell-death (apoptosis, autophagy, and mitophagy-related processes) pathways modulated by BBR. (E) GO enrichment analysis indicating involvement in apoptosis process, NF-κB and JAK-STAT signaling. (F) Protein–protein interaction network of DEPs in BBR vs H_2O_2, identifying HIF1A, BCL2L1, and NFKB1 as central hub proteins. (G) GSEA showed that BBR upregulated mucin-type O-glycan biosynthesis, peroxisome, and glycosaminoglycan biosynthesis, while downregulating RIG-I–like receptor signaling, Toll-like receptor signaling, and apoptosis.

Supplementary Files

This is a list of supplementary files associated with this preprint. Click to download.

- supplementaryTableS5ARRIVEchecklist.xlsx
- supplementarymaterials.docx
- GraphicalAbstract.jpg